

Modeling and Simulation of Multiple-Valued and Nonlinear Quantum Photonic Components

Joshua Ange*, Mason Tuller*, Jessie M. Henderson*, Elena R. Henderson*, Bradley A. Moores[†],
Duncan L. MacFarlane*, Mitchell A. Thornton*

**Darwin Deason Institute for Cyber Security, Southern Methodist University
Dallas, Texas, USA*

{jwange, mtuller, hendersonj, erhenderson, dmacfarlane, mitch}@smu.edu

[†]Leidos Corporation

Reston, Virginia, USA

Bradley.A.Moores@leidos.com

Abstract—Quantum computing using qudits of dimension higher than two can offer performance and application benefits beyond those when using standard, two-dimensional qubits. There is thus reason to develop higher-dimensional quantum computing hardware, including for photonic quantum computers. But unlike for qubit-based quantum computing, software for modeling higher-dimensional components is less developed and, for nonlinear quantum photonic components in particular, is effectively non-existent. We demonstrate how Cirq, Google’s quantum programming package that can simulate higher-dimensional quantum algorithms, can be leveraged as a multi-dimensional quantum photonic component design tool. Although Cirq is intended for superconducting quantum computers, its ability to work with user-specified unitary matrices having dimension greater than two allows for behavioral modeling of quantum photonic circuit components. Specifically, we show examples of modeling time-coincident entangled photon comb generators and electro-optic modulators as mixers for frequency-encoded quantum informatics.

Index Terms—quantum computing, photonics, Cirq, higher-dimensional, qudit

I. INTRODUCTION

Quantum photonic integrated circuit (QPIC) fabrication capability is rapidly emerging as several foundries offer services supporting a variety of processes and wavelengths. Many of these foundries provide Software Design Kits (SDK) with standard cell libraries that enable QPICs to be designed at fabless facilities.¹ Concurrently with these advances, design automation tools continue to improve; however, they are still restricted in capability when compared to classical electronic ASIC toolsets. Support for behavioral modeling is especially limited, particularly for nonlinear photonic components. The simulation tools commonly available to quantum photonic designers are either based upon partial differential equation (PDE) solvers or are models of interconnected components in terms of S-parameter matrices. While these tools are adequate for circuits comprised of a few components, computational complexity restricts scalability to even moderately sized circuits that can now be built given advances in QPIC fabrication

¹Meaning those that concentrate on designing chips, and not on fabricating them.

and the availability of SDKs for fabless designs. Therefore, there is a need for a high-level behavioral modeling capability that enables a designer to develop moderately large circuits with rapid iteration that requires only edge-device classes of computers.

Most quantum informatic behavioral modeling tools, such as TKET, Qiskit, Q#, QuantumSkynet, Cirq and others [1]–[5], support the discrete variable (DV) quantum computing (QC) paradigm. Some tools, such as Strawberry Fields [6] and PennyLane [7] from Xanadu Quantum Technologies, do support photonic QC with simulation capabilities, but Strawberry Fields is designed for continuous variable (CV) QC and is not applicable for the DV quantum photonic circuits we consider here. Furthermore, most of these tools are limited to simulating binary, or two-dimensional qubit gates only. Exceptions to the two-dimensional restriction are the Cirq and QuantumSkynet DV QC simulators.

To our knowledge, there are no behavioral-level simulators for quantum photonic circuits. To address this deficit in behavioral-level simulation of QPIC circuits with higher-dimensional and nonlinear components, we describe a method whereby the Cirq simulation tool can be used to simulate quantum photonic components—whether targeting table-top or QPIC implementations—without modifying Cirq source code.

Certain quantum photonic effects such as entanglement are typically accomplished with nonlinear components [8]. Furthermore, nonlinear components are also included in most QPICs because photons are highly non-interactive under linear operators. Nonlinear components are leveraged for phenomena such as parametric down-conversion (PDC) and four-wave mixing (FWM), which are used for several purposes and which can be implemented using certain crystalline materials such as as beta-barium borate or lithium niobate, resonant microrings, and EOM cells.

While it is relatively straightforward to use Cirq with linear photonic components such as beam splitters and phase shifters—a user needs only to characterize their behavior in terms of a unitary matrix—the implementation of nonlinear component models is not as obvious. In this paper, we simulate

certain microring and EOM nonlinear quantum photonic components using the linear transfer matrix descriptions available in the Cirq tool. We show how the concept of the diffusion operator, commonly used in Grover’s search algorithm, can be adapted to derive a cascade of unitary linear transfer matrices that provide a model with the required simulation response, and we present a method for representing arbitrary nonlinear transfer functions as a cascade of appropriately-initialized linear transfer matrices within the Cirq framework. We emphasize that although the resulting models may not be directly realizable if they do not correspond to known implementations of nonlinear devices, our method still behaviorally models the nonlinear QPIC components, allowing designers to explore high-level options before capturing lower-level abstractions.

One advantage of the approaches described here is that quantum photonic circuits may be simulated quickly, easily, and with fewer computational resources than would be required if designers resorted to using low-level partial differential equation (PDE) solvers. PDE solvers often require the time-consuming procedure of developing an appropriate, low-level geometric model, and the computational requirements of using those models often require enterprise-level computing resources. Even when such resources are available, they are often not practically scalable for large photonic circuits. Our methods only require the specification of behavioral-level transfer matrices thereby allowing for more efficient development of larger photonic circuitry.

II. BACKGROUND

In attempt to make this paper accessible, we briefly review background concepts and provide references for further review.

A. Frequency-bin Encoding

Energy is a quantum observable, and for quantum photonic circuit implementations, photon energy is directly proportional to frequency as $E_{\text{photon}} = \hbar\omega$. All quantum observables can be in a state of superposition before observation, meaning the wave function of a photon can be expressed as a superposition of multiple wavelengths leading to the interesting notion of a “multi-colored” photon. Frequency-bin information encoding for quantum photonic communications is very attractive given the maturity of classical optical components used in telecommunication applications such as “Wavelength Division Multiplexing” (WDM); the ability for multiple wavelengths to be in superposition allowing higher-dimensional quantum states; the allowance of room-temperature quantum photonics; and the fact that photons are true “flying qubits” [9].

Mathematically, a four-dimensional frequency-bin encoded quantum photonic state or wave function can be expressed as $|\Psi\rangle = a_0|0\rangle + a_1|1\rangle + a_2|2\rangle + a_3|3\rangle$ where each basis-ket corresponds to one of four superimposed wavelengths, $\{\omega_0, \omega_1, \omega_2, \omega_3\}$. An example quantum photonic communications system can be constructed using fiber optic cable for a channel and using transmitter and receiver circuitry that manipulates the superimposed frequencies within one or more photon’s wave functions. In a photonic architecture,

modification of the frequency content beyond amplitude and phase variation may only be performed with nonlinear devices.

B. Higher-dimensional Quantum Gates

For binary-dimensioned qubits, the Hadamard matrix evolves a single basis state into a superposition of all basis vectors, and its generalization in higher dimensions is the Chrestenson operation [10]–[12]. The four-dimensional Chrestenson operator, \mathbf{C}_4 , is given in Equation 1.

$$\mathbf{C}_4 = \frac{1}{\sqrt{4}} \begin{bmatrix} 1 & 1 & 1 & 1 \\ 1 & i & -1 & -i \\ 1 & -1 & 1 & -1 \\ 1 & -i & -1 & i \end{bmatrix} \quad (1)$$

The four-dimensional \mathbf{C}_4 gate implemented with frequency-bin encoding corresponds to a device that transforms a wave function comprising a single wavelength, a pure state of the form $|\Psi\rangle = |j\rangle$ for $j \in \{0, 1, 2, 3\}$, into a perfect superposition, $|\Psi\rangle = a_0|0\rangle + a_1|1\rangle + a_2|2\rangle + a_3|3\rangle$ where $a_j^* a_j = |a_j|^2 = \frac{1}{4}$.

The two-qudit “Controlled-Modulo-Add” gate is another useful operator; it is denoted as $\mathbf{A}_{h,k}$ where h is the activation value or the $|h\rangle$ component that causes the target qudit to be evolved. That evolution is application of a 4×4 transfer matrix that increases the value of each non-zero basis component by $k \pmod{4}$. The generalized transfer matrix for an r -dimensional gate of this form is given in Equation 2,

$$\mathbf{A}_{h,k} = \begin{bmatrix} \mathbf{D}_0 & \mathbf{0}_r & \cdots & \cdots & \cdots & \cdots & \mathbf{0}_r \\ \mathbf{0}_r & \mathbf{D}_1 & \mathbf{0}_r & \cdots & \cdots & \cdots & \mathbf{0}_r \\ \vdots & \mathbf{0}_r & \ddots & \mathbf{0}_r & \cdots & \cdots & \mathbf{0}_r \\ \vdots & \vdots & \mathbf{0}_r & \mathbf{D}_j & \mathbf{0}_r & \cdots & \mathbf{0}_r \\ \vdots & \vdots & \vdots & \mathbf{0}_r & \ddots & \mathbf{0}_r & \vdots \\ \vdots & \vdots & \vdots & \vdots & \mathbf{0}_r & \ddots & \mathbf{0}_r \\ \mathbf{0}_r & \mathbf{0}_r & \mathbf{0}_r & \mathbf{0}_r & \cdots & \mathbf{0}_r & \mathbf{D}_{(r-1)} \end{bmatrix} \quad (2)$$

where,

$$\mathbf{D}_i = \begin{cases} \mathbf{M}_0 = \mathbf{I}_r, & i \neq h \\ \mathbf{M}_k, & i = h \end{cases}$$

with \mathbf{M}_k representing the single qudit modulo-add- k transfer matrix as a permutation that is conditionally applied to the target qudit, depending on the state of the activation qudit.

C. QMUX, QROM, Kernel and Entanglement Generators

The general form of a four-dimensional quantum multiplexer (QMUX) is shown in Figure 1a where the uppermost qudit, $|\Psi\rangle$, can be considered the “control” and the lowermost qudit, $|\Phi\rangle$, can be considered the “data” since $|\Psi\rangle$ selects the target transfer matrix used to evolve $|\Phi\rangle$. The QMUX can also be considered an instance of a quantum read-only memory (QROM) where $|\Psi\rangle$ serves as the address qudit and $|\Phi\rangle$ as the data qudit [13]. For example, any arbitrary quantum state of the form $|\Omega_k\rangle = a_{0,k}|0\rangle + a_{1,k}|1\rangle + a_{2,k}|2\rangle + a_{3,k}|3\rangle$ can

be “stored” within a target unitary transfer matrix, \mathbf{U}_k , as a projector matrix of the form $\mathbf{U}_k = |\Omega_k\rangle\langle 0|$; the ancilla input $|\Phi\rangle$ can be initialized to $|0\rangle$; and the address qubit $|\Psi\rangle = |k\rangle$ can be used to choose which of the “stored” $|\Omega_k\rangle$ should be evolved. As is always the case with quantum circuits, a superposition of the quantum multiplexer data outputs can be computed by placing the control qudit, depicted as $|\Psi\rangle$ in Figure 1a, into an initial state of superposition. Figure 1b illustrates addition of an \mathbf{C}_4 gate to evolve $|\Psi\rangle$ into a state of superposition before the multiplexer. Figure 1c illustrates addition of a restoring \mathbf{C}_4 gate, which is useful in a variety of applications including in quantum machine learning applications [14].

Restricting the form of the target transfer matrices, \mathbf{U}_k , to be single-qudit Modulo-Add gates, \mathbf{M}_k , results in a higher-dimensional generalization of two-dimensional Bell state entanglement and detanglement circuits [12]. Figure 1d illustrates an example case of a four-dimensional entanglement generator: a two-qudit entangling circuit can be constructed with a \mathbf{C}_4 gate followed by a sequence of $\mathbf{A}_{h,k}$ gates (*i.e.*, controlled \mathbf{M}_k gates). Note that the case of $\mathbf{A}_{0,0}$ is not included since $\mathbf{A}_{0,0} = \mathbf{I}_{16}$. The omission of one or more $\mathbf{A}_{h,k}$ gates in Figure 1d results in a partial entanglement generator [12].

Circuits of the form in Figure 1 are a general and powerful way to construct quantum circuits with arbitrary transfer matrices in a manner analogous to classical switching circuits constructed as arrays of multiplexers or as stored switching-function truth tables in ROM circuits. Indeed, the synthesis of any desired algorithm can be accomplished as a cascade of circuits in the form of those in Figure 1 in a manner analogous to synthesizing classical switching functions with multiplexer or ROM circuits.

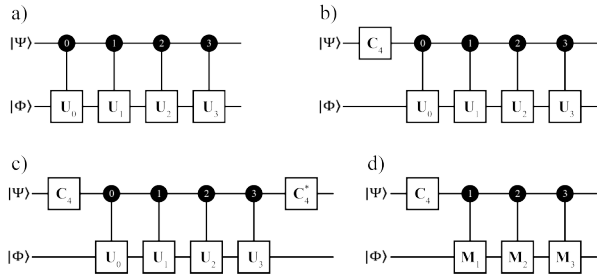


Fig. 1. QMUX, QROM & Entanglement generators for four-dimensional qudits.

D. Grover’s Search Algorithm

Our approach for modeling an entangled frequency-bin pair generator leverages the oracle and diffusion operator concepts from Grover’s search algorithm, and in the interest of space, we leave details to [15]–[17].

E. Entangled Photon Frequency Comb Generation

A ‘microring resonator’ (MRR) evanescently coupled to a waveguide is often used for the nonlinear optical production

of entangled signal-idler photon pairs since it can induce a FWM process. The MRR structure can be implemented within a QPIC wherein photons with single-basis frequency-bin wave functions of the form $|\Psi\rangle = |k\rangle$ are provided by a pump laser with wavelength ω_0 and coupled into the ring. The MRR is designed to have a circumference of $n \times \lambda$ where λ is the wavelength corresponding to ω_0 . This geometry enables the MRR to have multiple resonant frequencies located at $\pm N v_g / \lambda$, where v_g is the velocity of light in the material comprising the structure. A circular standing wave forms within the MRR as pump photons accumulate within the ring. Due to a nonlinear FWM process, some fraction of these photons decompose into a time-coincident pair referred to as a “signal” and an “idler” photon. The signal photon’s wave function comprises a superposition of frequency-bins spaced at $\Delta\omega$ intervals in the frequency domain given the total circumference of the ring, or alternatively, the MRR’s “Free Spectral Range” (FSR), $\omega_0 + N \times \Delta\omega$ where N is a positive integer. The FSR is the spacing between ring resonances, where the mode dwells longest in the ring. That long group delay time increases the probability of a spontaneous nonlinear collision event that produces frequency-entangled signal and idler photon pairs. Likewise, the idler photon’s wave function comprises a superposition of frequency-bins located at $\omega_0 - N \times \Delta\omega$. Thus, the total quantum state of the signal/idler pair forms a frequency comb [18]–[20]. A QPIC designer can complement a MRR-based frequency comb with a bandpass filter to limit the number of frequency-bins and thus set the dimension, D , to be the number of resonant MRR frequencies that fall within the filter passband. Additionally and importantly, the signal/idler photonic wave functions are entangled in frequency, such that changes to the signal photon’s probability amplitude at a specific frequency-bin, $\omega_0 + K \times \Delta\omega$, for some constant value of K , to also affect the idler’s image frequency-bin located at $\omega_0 - K \times \Delta\omega$.

F. Electro-optic Modulators

The EOM is a quantum photonic device that can be used for a variety of purposes and can be implemented as a QPIC component [8], [21], [22]. EOMs are particularly useful in quantum informatics applications that use frequency-bin encoding, because they can transfer energy from one frequency-bin to another in a photon’s wave function, which effectively modifies the probability amplitudes of the bases comprising the photon. Physically, EOMs operate using the electro-optic effect of a material to modulate the phase term of a photonic wave function with an externally-applied classical voltage signal thereby instantiating an electric field across the material. The applied voltage signal is typically time-varying in the radio frequency (RF) range [23] and changes the optical refractive index in a crystal. When the applied RF voltage is periodic with frequency, ω_{drive} , and the frequency component within a photon’s wave function is ω_0 , the EOM evolves the wave function to contain frequency components at $\omega_0 \pm N \times \omega_{drive}$ where N is an integer. While some of the generated frequencies may fall outside the discrete and finite

set of frequencies selected by the QPIC designer to represent information, they can be removed by coupling the output of the EOM to passband filters that move energy from the unwanted frequency components back into the desired frequency bins of the photonic wave function.

EOMs are often used in quantum photonic informatics circuits to apply an RF sine wave voltage with a photonic wave function comprised of a single basis wavelength, ω_0 (e.g., a pump laser operating at ω_0). In this case, the EOM can be viewed as generating sidebands within the wave function, thereby increasing its optical bandwidth. The resulting wave function, assuming an idealized EOM, contains energy in discrete frequency bins that span $N \in \{-\infty, +\infty\}$ but where the amplitudes vary according to the Jacobi-Anger expansion of $e^{-iz\cos(\theta)}$ in terms of Bessel functions of the first kind, $J_N(z)$, as given in Equation 3.

$$e^{-iz\cos(\theta)} = \sum_{N=-\infty}^{\infty} (-i)^N J_N(z) e^{-iN\theta} \quad (3)$$

III. MODELING COMPONENTS WITH CIRQ

A. Cirq Overview

Cirq is a Python library that allows for specifying quantum circuits at the transfer matrix level and executing circuits on quantum hardware or simulators. Quantum gates can be specified by directly providing transfer matrices, including for D -dimensional qudits, which allows for modeling systems based on photonic, superconducting semiconductor, or any of a variety of technologies. For the application of interest here, DV quantum photonics, some allowable gate operators within the Cirq environment do not reflect physical reality. For example, specification of deterministic multi-qudit controlled-gates is possible in Cirq, but because of the difficulty of achieving interaction between two photons is extremely difficult to realize in actual circuitry. However, we can use such controlled-gates in the construction of behavioral models for nonlinear quantum photonic components.

B. Frequency Comb Generator Model

As previously described, an MRR with appropriate tuning and filtering components can be used to implement a signal/idler pair of photons whose wave functions comprise a superposition of entangled frequency bins. One such circuit is shown in Figure 2a: a single photon pump laser operating at wavelength ω_0 produces time-coincident signal/idler pairs [24], [25]. Figure 2b shows the energy content of the signal/idler pairs in the frequency domain. This design provides increased tunability since the feed and drop waveguides that couple photons into and out of the MRR each have two symmetric-point coupling regions with the MRR. This forms Mach-Zender Interferometer (MZI) structures that, with the addition of electrical thermal heating components (not shown), allow for controllable variability in the position of the frequency bins in the photonic wave functions.

As shown in Figure 2a, the MRR structure is excited by coupling a pump photon source to the “add” port. Because

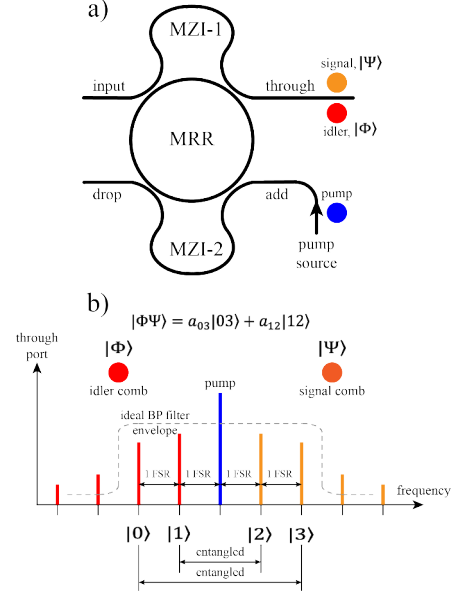


Fig. 2. 4-dimensional entangled pair generation: (a) MRR-based implementation with dual MZI for tuning and, (b) Frequency spectrum of the 2-photon quantum state, $|\Phi\Psi\rangle$.

Cirq is designed for QC circuit specifications, the total number of qudits must be declared. Instead of declaring a single qudit as the wave function of a single pump photon with energy equal to $\hbar\omega_a$, we initialize the signal/idler pair wave functions that will be produced as $|\Psi\Phi\rangle = |00\rangle$. We note that $|\Psi\Phi\rangle$ could be initialized to any arbitrary single basis vector without loss of generality in our modeling approach.

Next, to generate all possible frequency components in equal superposition, we apply a four-dimensional Chrestenson operator, C_4 , to both $|\Phi\rangle$ and $|\Psi\rangle$. At this point, each qudit contains a perfect superposition of all possible frequency components in the four-dimensional spectrum, which is not true of the physical functionality of the MRR circuit, because it is impossible for the idler wave function to emerge with frequency components greater than the pump frequency, ω_0 , and likewise, the signal wave function cannot contain frequency components less than ω_0 . Therefore, the next step is to remove the undesired frequency components in $|\Psi\Phi\rangle$, and we do so using Grover’s oracle and diffusion filters as previously discussed. Using the oracle development approach of [17], we create a unitary matrix that selects the desired frequencies and we label this operator as “wavelength select.” Because the wavelength select transfer matrices vary in structure depending on the desired frequencies, we developed a Python script that receives the dimension and desired wavelengths as input and then computes the corresponding wavelength select matrix as output.

The wavelength select operator applies a “marking” process to the desired frequencies by applying a 180° phase shift to the desired frequencies in the input spectrum. In physical, QPIC terms, this procedure is a simple example of dispersion

management. Following the wavelength select operators, we apply diffusion filters that amplify the magnitudes of the probability amplitudes corresponding to the “marked” frequencies and attenuate the magnitudes of the unmarked frequencies via the “inversion about the mean” approach of [15], [17]. Wavelength select and diffusion filters are applied iteratively, with successive iterations providing additional amplification and attenuation. However, as discussed in [16], using too many iterations can cause undesirable effects whereby amplification/attenuation from a previous stage is actually reversed. For the examples in this work, we experimentally decided to apply two iterations.

Figure 3a depicts the Cirq model in the form of a cascade of linear operators. This model was configured with appropriate wavelength select and diffusion operators to produce the state $|\Psi\Phi\rangle = a_{03}|03\rangle + a_{12}|12\rangle$ using the Cirq simulator. Projective measurements were added to the outputs of the model of Figure 3a, and Figure 3b illustrates simulation results for 100,000 shots. Ideally, $|a_{03}|^2 = |a_{12}|^2 = \frac{1}{2}$ for perfect superposition among the two basis functions, but some error is present in the simulation results due to two predominant factors. First, the finite number of shots, results in sampling error since the probability amplitudes are estimated. Second, applying wavelength select and diffusion filters is—just like Grover’s search—a heuristic approach and not a theoretically-errorless solution. With 100,000 shots, we see that the largest occurrence of the undesired basis vector, $|21\rangle$, when compared to basis state $|12\rangle$ is still attenuated by approximately 17.5 dB.

C. Electro-Optic Modulator Model

Our EOM model operates as a mixer that generates all possible harmonic sidebands and images about a single input frequency. This can be realized by driving the EOM with an RF sinusoid at a chosen frequency ω_{drive} that yields frequency bins matching those of the MRR FSR. The exact value of ω_{drive} is obfuscated in our Cirq behavioral models since we compute with quantum state functions wherein the actual frequency-bin values are represented by the qudit basis, $\{|0\rangle, |1\rangle, |2\rangle, |3\rangle, \dots\}$. In keeping with our DV two-photon, signal/idler approach, the EOM model has two input qudits, $|\Psi\Phi\rangle$, and the output wave function contains all the side bands and their images. The EOM model is inspired by the combined concepts of the QROM [13] and high-dimensional bipartite entangled state generators [12]. The idea is to initially generate all possible superpositions of the input signal qudit, $|\Psi\rangle$, with a Chrestenson gate specified as a C_4 operator in the Cirq model file. The resulting superpositions may contain as few as a single frequency bin when the input $|\Psi\rangle$ state is already in a perfect superposition, or as many as all possible superpositions when the input $|\Psi\rangle$ state is in the collapsed form of a single basis vector.

From the viewpoint of a QROM, the result of $C_4|\Psi\rangle$ is the “address” qudit accessing the memory where the EOM output response for a particular overall input state, $|\Psi\Phi\rangle$, is stored. Instead of using arbitrary unitary matrices, U_k , as the target single-qudit transformations of $|\Phi\rangle$, we note that the

desired frequency-bin sidebands should be integer multiples of the input frequency bins represented by the initial state, $|\Psi\Phi\rangle$. By restricting the U_k target transfer matrices to be Modulo-Add transfer matrices, we ensure that the produced sidebands are integer multiples of the FSR of a preceding MRR stage. So, the location of the non-zero values of the M_k matrices can be understood to physically correspond to the choice of RF drive frequency and its relation to the separation between frequencies of the multicolor photons in play.

We assume that the input state, $|\Psi\Phi\rangle$, comprises bases consistent with the discrete frequency-bins dictated by a preceding MRR’s FSR, but such a state can still be in the form of an arbitrary wave function. Consequently, we did not find a universal EOM model, but rather a non-unique family of EOM models when the qudit dimension is restricted to $D = 4$. Note that, in Figure 4a, the cascade of C_4 gates has a restoring effect on the upper qudit. But there are some input states for which we found no model using both M_k gates and the constraints on the input state, so while it is possible that unitary matrices exist for such a QROM structure, we opted to prepare more complex EOM models—shown in Figure 4b—for these situations, involving additional M_k and C_4 gates. The resulting six EOM models are color-coded based on which should be used in a simulation for an input state of the form $|\Psi\Phi\rangle = a_{jk}|jk\rangle + a_{pq}|pq\rangle$. Figure 4c is a “lookup” table with the row input jk corresponding to $|jk\rangle$ and the column input pq corresponding to $|pq\rangle$.

As an example of the simulation results, we consider an arbitrary case where the input state to the EOM is $|\Psi\Phi\rangle = \frac{1}{\sqrt{2}}|03\rangle + \frac{1}{\sqrt{2}}|12\rangle$. After generating this input state using the approach of Section III-B, we applied the “blue” model of Figure 4b and simulated it with 100,000 shots to produce Figure 3c, which executed in 5-10 seconds on a laptop computer. While the distribution envelope of Figure 3c does not vary in accordance with the Jacobi-Anger distribution as would occur in an actual physical implementation, this can be remedied by adding wavelength select and diffusion filters to manipulate the probability amplitudes of the EOM output state.

IV. CONCLUSIONS AND FUTURE WORK

This work presents a method for behavioral simulation of nonlinear quantum photonic components using the DV QC simulator Cirq with specific examples of a tunable microring resonator excited by a single photon laser source and an electro-optic modulator configured to act as a frequency mixer. Future work will investigate models of other common structures and optimize the models described here.

REFERENCES

- [1] S. Siverajah, S. Dilkes, A. Cowtan, and R. Duncan, “[t|ket]: a retargetable compiler for NISQ devices,” *Quantum Science and Technology*, vol. 6, no. 014003, p. 28, 2021.
- [2] IBM. Qiskit. [Online]. Available: <https://www.ibm.com/quantum/qiskit>
- [3] Microsoft. Introduction to the quantum programming language Q#. [Online]. Available: <https://learn.microsoft.com/en-us/azure/quantum/qsharp-overview>

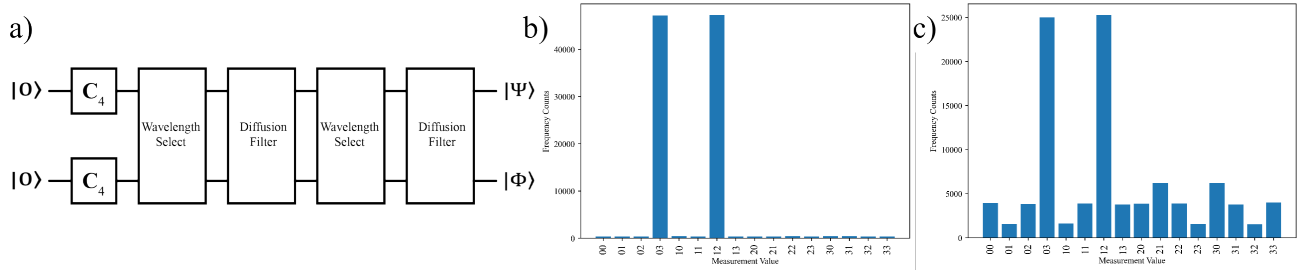


Fig. 3. (a) 4-dimensional comb generator model for $|\Psi\Phi\rangle$. (b) Cirq model results for the MRR-based comb generator model for $|\Psi\Phi\rangle$. (c) Cirq model results for the EOM for input state $|\Psi\Phi\rangle = a_{03}|03\rangle + a_{12}|12\rangle$ from frequency comb generator.

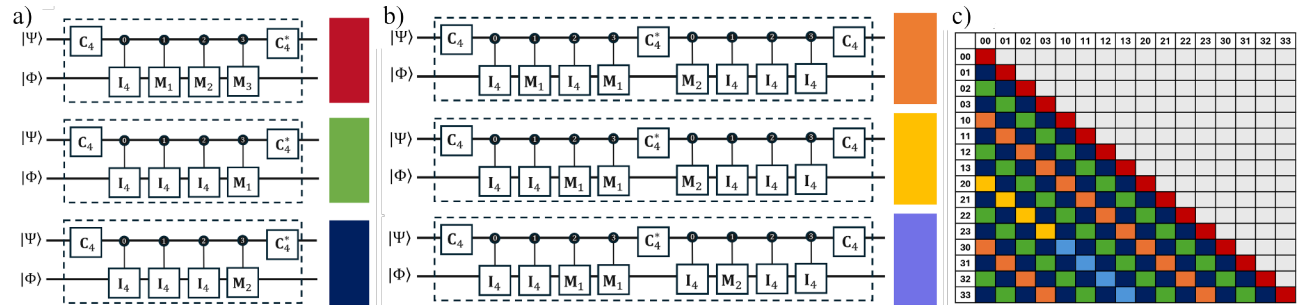


Fig. 4. (a) “Simple” and (b) “Complex” Cirq models of the EOM. (c) A color-coded “lookup” of EOM models for a quantum state consisting of a superposition of two states.

- [4] A. Giraldo-Carvajal and J. A. Jaramillo-Villegas, “QuantumSkynet: A high dimensional quantum computing simulator,” in *Frontiers in Optics*. Optica Publishing Group, 2020, pp. JW6A–25.
- [5] Cirq Developers, “Cirq,” 2024. [Online]. Available: <https://zenodo.org/records/11398048>
- [6] N. Killoran, J. Izaac, N. Quesada, V. Bergholm, M. Amy, and C. Weedbrook, “Strawberry Fields: A software platform for photonic quantum computing,” *Quantum*, vol. 3, p. 129, 2019.
- [7] V. Bergholm, J. Izaac, M. Schuld, C. Gogolin, S. Ahmed, V. Ajith, M. S. Alam, G. Alonso-Linaje, B. AkashNarayanan, A. Asadi, and *et al.*, “Pennylane: Automatic differentiation of hybrid quantum-classical computations,” *arXiv preprint arXiv:1811.04968*, p. 18, 2022.
- [8] J. Capmany and C. Fernández-Pousa, “Quantum modelling of electro-optic modulators,” *Laser & Photonics Reviews*, vol. 5, no. 6, pp. 750–772, 2011.
- [9] H.-H. Lu, M. Liscidini, A. L. Gaeta, A. M. Weiner, and J. M. Lukens, “Frequency-bin photonic quantum information,” *Optica*, vol. 10, no. 12, pp. 1655–1671, Dec 2023.
- [10] K. N. Smith, T. P. LaFave Jr, D. L. MacFarlane, and M. A. Thornton, “Higher-radix Chrestenson gates for photonic quantum computation,” *Journal of Applied Logics-IFCOLOG Journal of Logics and Their Applications*, vol. 5, no. 9, pp. 1781–1798, 2018.
- [11] K. N. Smith, T. P. LaFave, D. L. MacFarlane, and M. A. Thornton, “A radix-4 Chrestenson gate for optical quantum computation,” in *48th International Symposium on Multiple-Valued Logic (ISMVL)*. IEEE, 2018, pp. 260–265.
- [12] K. N. Smith and M. A. Thornton, “Higher dimension quantum entanglement generators,” *ACM Journal on Emerging Technologies in Computing Systems (JETC)*, vol. 16, no. 1, pp. 1–21, 2019.
- [13] A. Sinha, E. R. Henderson, J. M. Henderson, and M. A. Thornton, “Automated quantum memory compilation with improved dynamic range,” in *Workshop on Quantum Computing Software (QCS22)*. ACM and IEEE, 2022, p. 14.
- [14] A. Sinha and M. A. Thornton, “Quantum multiple valued kernel circuits,” in *52nd International Symposium on Multiple-Valued Logic (ISMVL)*. IEEE, 2022, pp. 1–8.
- [15] L. Grover, “A fast quantum mechanical algorithm for database search,” in *Symposium on the Theory of Computing (STOC)*. ACM, 1996, pp. 212–218.
- [16] J. M. Henderson, E. R. Henderson, A. Sinha, D. M. Miller, and M. A. Thornton, “Automated quantum oracle synthesis with a minimal number of qubits,” in *Quantum Information Science, Sensing and Computation XV*. SPIE, 2023, p. 1251706.
- [17] E. Acar, S. Gündüz, G. Akpinar, and İ. Yılmaz, “High-dimensional Grover multi-target search algorithm on Cirq,” *The European Physical Journal Plus*, vol. 137, no. 2, p. 244, Feb 2022.
- [18] W. Bogaerts, *et al.*, “Silicon microring resonators,” *Laser Photonics*, vol. 6, no. 1, pp. 47–73, 2012.
- [19] Y. R. Bawankar and A. Singh, “Microring resonators based applications in silicon photonics – a review,” in *Conference on Information and Communication Technology (CICT)*. IEEE, 2021, pp. 1–6.
- [20] A. Mirza, *et al.*, “Silicon photonic microring resonators: A comprehensive design–space exploration and optimization under fabrication-process variations,” *IEEE Transactions on CAD*, vol. 41, no. 10, pp. 3359–3372, 2022.
- [21] T. A. Maldonado, “Chapter 13, Electro-Optic Modulators,” in *Handbook of Optics, Volume II Devices, Measurements, & Properties*, M. Bass, E. W. VanStryland, D. R. Williams, and W. L. Wolfe, Eds. Orlando, Florida, USA: McGraw-Hill, 1995, pp. 446–480.
- [22] G. Sinatkas, T. Christopoulos, O. Tsilipakos, and E. E. Kriezis, “Electro-optic modulation in integrated photonics,” *Journal of Applied Physics*, vol. 130, p. 010901, 2021.
- [23] P. Kolchin, C. Belthangady, S. Du, G. Y. Yin, and S. E. Harris, “Electro-optic modulation of single photons,” *Phys. Rev. Lett.*, vol. 101, p. 103601, Sep 2008.
- [24] L. Chen, N. Sherwood-Droz, and M. Lipson, “Compact bandwidth-tunable microring resonators,” *Optics Letters*, vol. 32, no. 22, pp. 3361–3363, 2007.
- [25] Z. Vernon, M. Menotti, C. C. Tison, J. A. Steidle, M. L. Fanto, and *et al.*, “Truly unentangled photon pairs without spectral filtering,” *Optics Letters*, vol. 42, no. 18, pp. 3638–3641, 2017.